IOP Conf. Series: Materials Science and Engineering **301** (2018) 012108 doi:10.1088/1757-899X/301/1/012108

Thermal Decomposition Synthesis of Graphene Nanosheets Anchored on Mn_3O_4 Nanoparticles as Anodes in Lithium Ion Batteries

Xihao Tang[a], Xiao Ma[a], Danfeng Qiu*[a], Gang Bu[a], Yongjun Xia[a], Bin Zhao[b], Zixia Lin[b] and Yi Shi[b]

[a]Key Laboratory of Radar Imaging and Microwave Photonics (Nanjing Univ. Aeronau t. Astronaut.), Ministry of Education, College of Electronic and Information Engineeri ng, Nanjing University of Aeronautics andAstronautics, Nanjing, 210016, China
[b]National Laboratory of Microstructures and School of Electronic Science and Engineering, Nanjing University, Nanjing, China
E-mail: dfqiu@nuaa.edu.cn

Abstract. Graphene nanosheets (GNS) anchored on Mn_3O_4 nanoparticles have been successfully synthesized through in situ thermal decomposition of Mn $(NO_3)_2$ without the use of any templates or surfactants. Mn_3O_4 particles were coordinately distributed on the GNS surface. This was achieved by forming 3D nanostructures to avoid detrimental graphene layer stacking, and was characterized using a scanning electron microscope. The Mn_3O_4/GNS nanocomposite delivers an initial capacity of 1450 mAh g^{-1} at a current density of 100 mA g^{-1}. It also maintains a high reversible capacity of 930 mAh g^{-1} even after 60 charge-discharge cycles without showing any apparent decay.

1. Introduction

Lithium ion batteries (LIBs) have long been considered as an attractive power source for a wide variety of applications such as mobile phones, laptops, and electric vehicles. This is because of the high energy and power densities as well as the long cycle lifetime of LIBs [1-4]. However, the commercial anode material of graphitic carbon could not meet the high power and energy density requirements of next-generation LIBs because of its relatively low capacity of 372 mAh g^{-1}, low security, and poor cycling stability and rate capability [5-7]. Transition metal oxides such as Co_3O_4 [8], SnO_2 [9], Fe_2O_3 [10], NiO [11], and Mn_3O_4 [12], have attracted more applications because of their extremely high reversible capacities and high energy densities. Among these materials, Mn_3O_4 attracts widespread interest for LIB applications because of its low price, nontoxic property, and high theoretical capacity [13-16]. However, transition metal oxides in practical applications always suffer from severe pulverization resulting from volume hyperbolic inflation during the charge-discharge process, which disastrously leads to rapid decay of capacity [17-19]. Additionally, low intrinsic electric conductivity further obstructs the application of Mn_3O_4 in batteries. To overcome these problems, numerous strategies have been developed to solve the intrinsic drawbacks of using Mn_3O_4. Conductive carbonaceous material/manganese oxide composites, such as amorphous carbon [20], carbon nanotubes (CNT) [21], graphite oxide (GO) [22], and graphene [23], have been used to improve the mechanical properties and electrical conductivity of Mn_3O_4 when it is used as an electrode. Among these carbon materials, graphene is an excellent substrate to host active nanomaterials for energy applications because of its high conductivity, large surface area, flexibility, mechanical

strength, light weight, and chemical stability. These properties greatly improve lithium ion diffusion kinetics. Meanwhile, the 3D GNS network and porous structure offer a highly conductive pathway for electrons and enable electrolyte to access the Mn_3O_4 anode material easily. Thus, the 3D-structured Mn_3O_4/GNS nanocomposite plays an important role in enhancing electrochemical performance and stability.

2. Experimental

GO was synthesized from natural graphite powders (universal grade, 99.985%) according to Hummers' method [24, 25], with slight modifications. The as-prepared GO was thermally exfoliated at 300 ℃ in air for 3 min and was subsequently treated in Ar at 900 ℃ for 3 h to obtain GNS [26]. In a typical synthesis of Mn_3O_4/GNS nanocomposite, 1074 mg of $Mn(NO_3)_2$ aqueous solution (50%) is mixed with 50 mL ethanol. A total of 55 mg of GNS was added into the solution and was ultrasonically treated for 10 min. The suspension solution was mixed using a magnetic stirrer in a ventilation cabinet. The ethanol in the solution evaporated continuously. The dried $Mn(NO_3)_2$/GNS composite was collected and treated in air at 200 ℃ for 10 h. $Mn(NO_3)_2$ was transformed in to Mn_3O_4. The relevant mechanism may be illustrated as follows:

$$3Mn(NO_3)_2 \rightleftharpoons Mn_3O_4 + 6NO_2 + O_2 \quad (1)$$

The final Mn_3O_4 content in Mn_3O_4/GNS is about 80% by weight. In the control experiments, simplex Mn_3O_4 sample was prepared by heating a $Mn(NO_3)_2$ aqueous solution (50%) in air at 200 ℃ for 10 h. The obtained samples were investigated using X-ray diffraction (XRD), scanning electron microscopy (SEM), and transmission electron microscopy (TEM). Electrochemical measurements were performed using 2032- type coin cells. A 90 wt% active material and 10 wt% *N*-methylpyrrolidone was also used. The obtained slurry was pasted on a copper foil and dried in vacuum. Coin cells were assembled in an Ar-filled glove box using an active material as the working electrode, a Li foil as the counter electrode, 1 M $LiPF_6$ in ethylene carbonate and diethyl carbonate (1:1 vol), and Celgard2250 as the separator. Charge-discharge measurements were carried out galvanostatically over a voltage range of 0.01–3 V using a battery testing system (LAND, Wuhan Jinnuo Electronics). The electrode tap density is 2 g cm^{-3}.

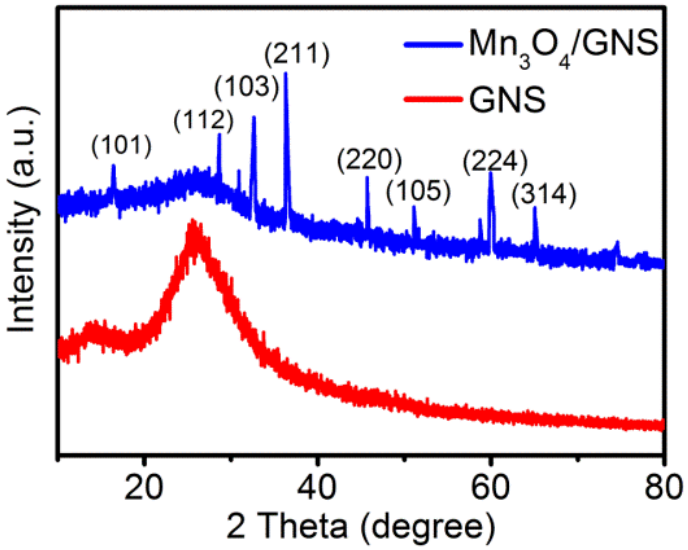

Figure 1. XRD patterns of the samples

3. Results and Discussion

XRD patterns of the Mn_3O_4/GNS nanocomposite and Mn_3O_4 particles are shown in Fig. 1. Diffraction peaks at the sample reflections are in good agreement with the standard pattern of the tetragonal Mn_3O_4 (JCPDS file no. 80-0382). No other phases or impurities were detected in the patterns. The broad peak at about 25 °C was the diffraction peak from the GNS sample's multilayer graphene.

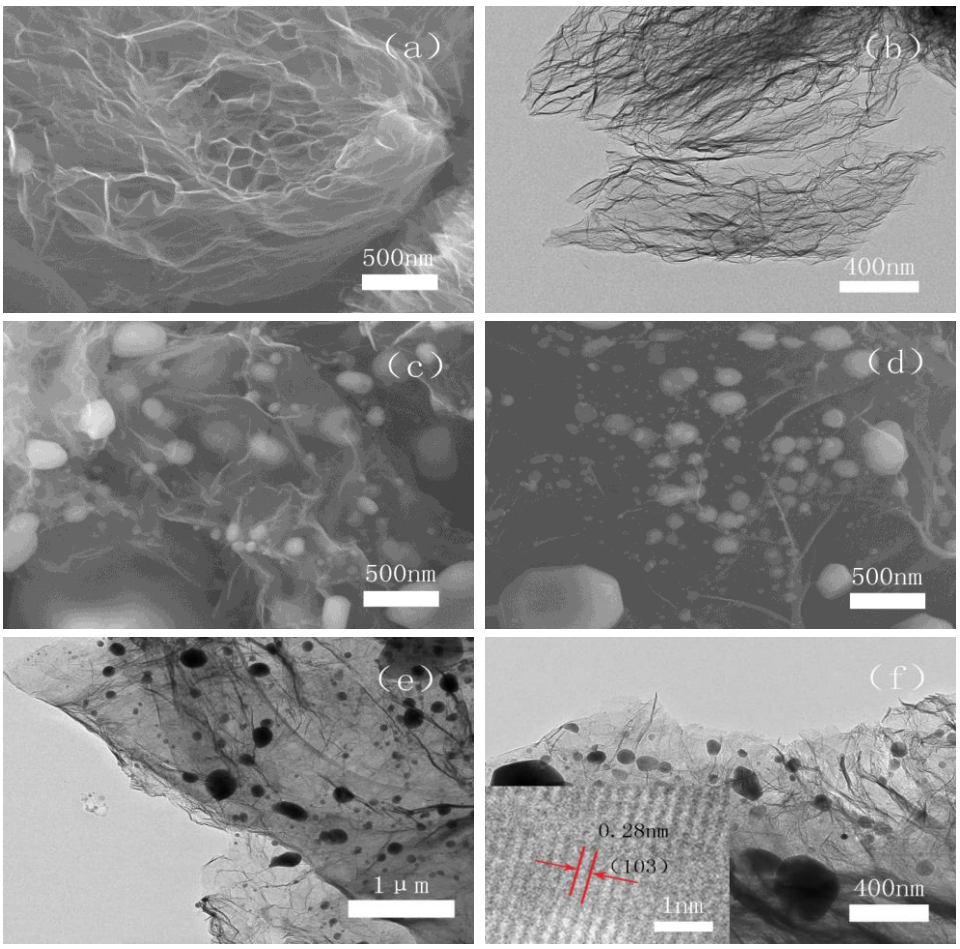

Figure 2. SEM (a) and TEM (b) images of GNS; SEM (c and d) and TEM (e and f) images of Mn_3O_4/GNS, inset: particle size distribution of Mn_3O_4 nanoparticles; High resolution TEM (f) images of Mn_3O_4/GNS.

The morphologies of as-prepared GNS and Mn_3O_4/GNS were examined using SEM and TEM. Figs. 2a and 2b show typical SEM and TEM images of the GNS sample. The GNS sample has a nanosheet structure, which results from the decomposition of GO's oxygen-containing groups during thermal exfoliation. In particular, the SEM images show numerous macropores among the nanosheets; these macropores facilitate the combination of $Mn(NO_3)_2$ and GNS. Figs. 2c and 2d show the SEM images of Mn_3O_4/GNS under different magnifications. Mn_3O_4 nanoparticles with diameters ranging from 20 nm to 500 nm tightly integrated with GNS. Figs. 2e and 2f show the TEM images of Mn_3O_4/GNS, revealing the firm attachment of Mn_3O_4 nanoparticles to GNS even after ultrasonication, which was done to disperse the sample for TEM observation. High resolution TEM was also used to confirm the interaction between Mn_3O_4 nanoparticles and GNS layers of the as-synthesized Mn_3O_4/GNS nanocomposite. In Fig. 2f, the lattice fringes with a spacing of 0.241 nm corresponds to the interplanar spacing of the (111) crystal plane of monoclinic Mn_3O_4. The electrochemical properties of bulk Mn_3O_4 and as-prepared Mn_3O_4/GNS nanocomposite electrode were investigated using CV over a range of 0.01 V to 3.0 V, as shown in Fig. 3. Fig. 3a shows the charge and discharge curves of the Mn_3O_4/ GNS

electrode run for one and two cycles at 100 mA g^{-1}. The first discharge curve of Mn_3O_4/GNS shows a voltage plateau at about 0.5 V. During the second circle, a quick drop in potential to about 1.2 V is observed, followed by a long voltage plateau between 1.2 V and 0.7 V. This voltage plateau is a result of two reactions, one of which is from the conventional reaction of Mn_3O_4:

$$Mn_3O_4 + 8Li \rightleftharpoons 3Mn + 4Li_2O \quad (2)$$

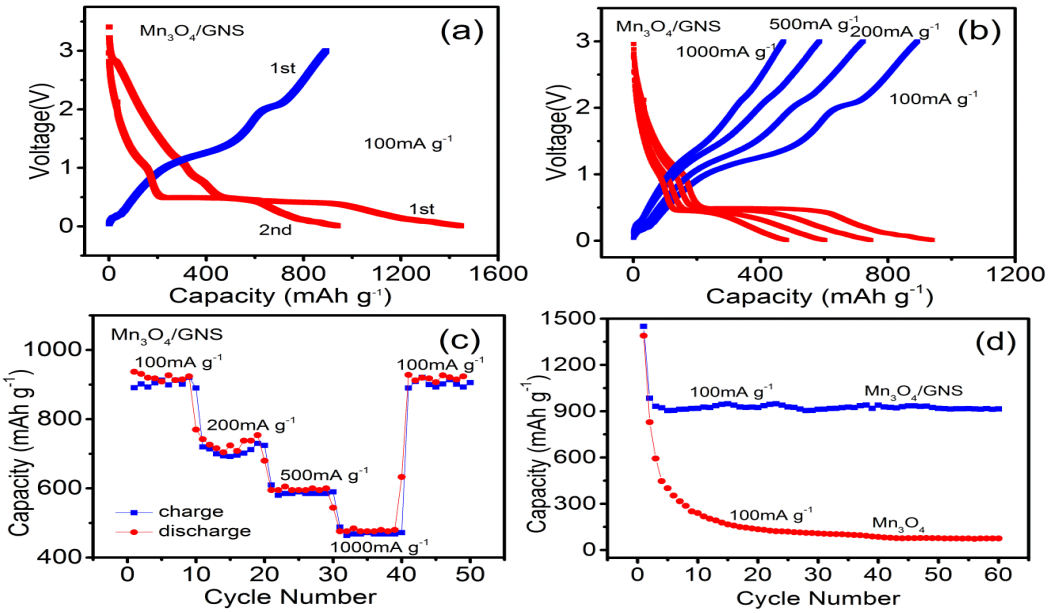

Figure 3. (a) Charge-discharge curves of Mn_3O_4/GNS for the first and second cycles at a current density of 100 mA g^{-1}; (b) representative charge-discharge curves of Mn_3O_4/GNS at various current densities; (c) capacity retention of Mn_3O_4/GNS at various current densities; and (d) discharge capacity retention of Mn_3O_4/GNS and simplex Mn_3O_4 at a current density of 100 mA g^{-1}

The other is from the reaction of GNS with Li. Fig. 3b shows representative charge and discharge curves of Mn_3O_4/GNS at various current densities. With the increase of current density, the charge potential of Mn_3O_4/GNS increased and the discharge potential decreased, rendering higher overpotential. The cell was first cycled at a low current density of 100 mA g^{-1} for 10 cycles, where a stable specific capacity of about 930 mAh g^{-1} (Fig. 3c) was obtained. The capacity was as high as 600 mAh g^{-1} after the current density was increased five times; nevertheless, the theoretical capacity of graphite (372 mAh g^{-1}) was still higher. Even at a high current density of 1,000 mA g^{-1}, more than 40% of the capacity can be retained. A capacity of about 930 mAh g^{-1} was retained after 60 cycles of charge and discharge at various current densities (Fig. 3c), indicating good cycling stability. Fig. 3d shows the charge-discharge capacity curves of the electrodes made of Mn_3O_4/GNS versus the cycle number under a charge-discharge current density of 100 mAh g^{-1} at 25 ℃. The specific discharge capacity of the Mn_3O_4/GNS composite is about 930 mAh g^{-1}, which is more than twice that of graphite, even after 60 cycles. In the case of pure Mn_3O_4, under a charge-discharge current density of 100 mA g^{-1}, only 100 mAh g^{-1} was retained by the electrode after 60 cycles. This result indicates that graphene-loaded Mn_3O_4 nanoparticles feature improved cycling stability. Mn_3O_4 nanoparticles integrated tightly with GNS.

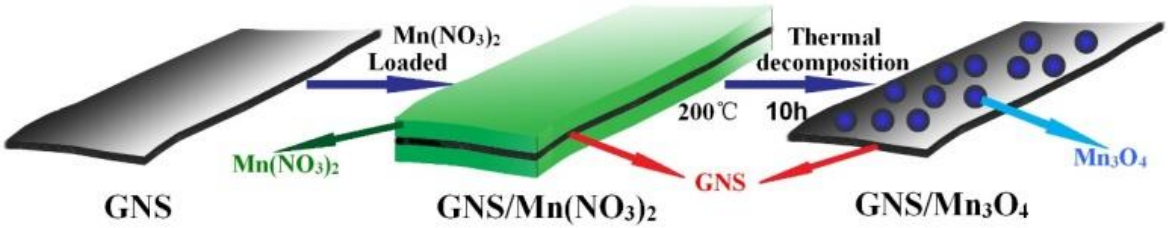

Figure 4. Schematic illustration of the Mn_3O_4/GNS nanocomposite

Fig. 4 schematically illustrates the typical synthesis of Mn_3O_4/GNS nanocomposite material. The high capacitance, good cycle performance, and excellent rate capability delivered in the case of the Mn_3O_4/GNS composite electrode can be explained by the several factors. First, the flexible GNS provided high electrical conductivity throughout the electrode and served as a mechanically strong framework, favoring long-term electrochemical stability and excellent rate performance. Second, well-dispersed Mn_3O_4 nanoparticles anchored on the GNS can significantly improve the electrochemical utilization of Mn_3O_4 and hence minimize the transport length of Li^+ during the charge-discharge process. Third, the graphene prevents aggregation of the Mn_3O_4 nanoparticles, preserving the high interfacial area between the Mn_3O_4 nanoparticles and the electrolyte. As a result, the nanocomposite had a large lithium storage capacity, excellent cyclic stability, and good rate capability. The results present a promising method for the synthesis of graphene-based nanocomposite and an interesting nanostructured system for LIB electrode materials that undergo large volume changes during cycling.

4. Conclusion

A one-step thermal decomposition method was developed to fabricate 3D-nanostructured Mn_3O_4/GNS nanocomposite as anodes of LIBs with enhanced energy density and sustained electrochemical stability. Through the co-precipitation method under high pressure and temperature, Mn_3O_4 particles were distributed uniformly amongst graphene layers, which was confirmed using SEM. GNS wrapped on the Mn_3O_4 particles to avoid severe expansion during the charge-discharge process. At the same time, such inserted Mn_3O_4 nanoparticles prevented severe stacking of graphene layers, hence forming a 3D structure with more active surface area to facilitate the diffusion of electrons and transport of lithium ions.

5. Acknowledgements

This work was supported by the National Natural Science Foundation of China (No. 61471195), the Fundamental Research Funds for the Central Universities (Nos. NJ20150017 and NS2014040), and 973 Project (Grant No. 2013CB932900).

6. References

[1] Dunn B, Kamath H and Tarascon J M 2011 Tarascon. Science **334** 928.
[2] Goodenough J B and Kim Y 2010 Chem Mater 22 587
[3] Yang S b, Feng X L, Wang X C, Tang K Maier and Müllen K 2010 *Angew Chem Int Ed* **49** 4795
[4] Liu C, Li F, Ma L P and Cheng H M 2010 *Adv Mater* **22** 28
[5] Augustyn V, Simon P and Dunn B 2014 *Environ E. Sci* **7** 1597
[6] Honma I, Yoo E, Kim J, Hosono E, Zhou H and Kudo T 2008 *Nano Lett* **8** 2277
[7] Wang J G, Zhang C B and Kang F Y 2015 *ACS Appl Mater Interfaces* **7** 9185
[8] Xu J M, Wu J S, Luo L L, Chen X Q, Qin H B, Dravid V, Mi S B and Jia C L 2015*J Power Sources* **274** 816.
[9] Paek S M, Yoo E and Honma I 2009 *Nano Lett* **9** 72
[10] Du M, Xu C H, Sun J and Gao L 2012 *Electrochim Acta* **80** 302
[11] Qiu D F, Xu Z J, Zheng M B, Zhao B, Pan L J, Pu L and Shi Y 2012 *Solid State Electron* **16** 1889

[12] Wang H L, Cui L F, Yang Y, Casalongue S, Robinson J T, Liang Y Y, Cui Y and Dai H J 2010 *J Am Chem Soc* **132** 13978
[13] Ayhan I A, Li Q, Meduri P, Oh H, Bhimanapati G R, Yang G, Robinson J A and Wang Q 2016 *RSC Adv* **6** 33022
[14] Augustyn V, Simon P and Dunn B 2014 *E. Environ. Sci* **7** 1597
[15] Tang H, Sui Y X, Zhu X Q and Bao Z H 2015 *Nanoscale Res Lett* **10** 260
[16] Wang J G, Zhang C B and Kang F Y 2015 *ACS Appl Mater Interfaces* **7** 9185.
[17] Arico A S, Bruce P, Scrosati B, Tarascon J M and Schalkwijk W V 2005 *Nat* Mater **4** 366.
[18] Roy P and Srivastava S K 2015 *J Mater Chem* **3** 2454
[19] Qiu D F, Bu G, Zhao B, Lin Z X, Pu L, Pan L J and Shi Y 2014 *Mater Lett* **119** 12
[20] Huang S Z, Cai Y, Jin J, Liu J, Li Y, Yu Y, Wang H E, Chen L H and Su B L 2015 *Nano Energy* **12** 833.
[21] Park S H and Lee W J 2015 *J Power Sources* **281** 301
[22] Wang Y J 2015 *J Mater Res* **30** 484.
[23] Raj B G S, Ramprasad R N R, Asiri A M, Wu J J and Anandan S 2015Electrochim *Acta* **156** 127
[24] Hummers W S and Offeman R E 1958 *J Am Chem Soc* **80** 1339
[25] Liu P G, Gong K C, Xiao P and Xiao M 2000 *J Mater Chem* **10** 933
[26] Du Q L, Zheng M B, Zhang L F, Wang Y W, Chen J H, Xue L P, Dai W J, Ji G B and Cao J M 2010 *Electrochim Acta* **55** 3897